Supplemental Figures

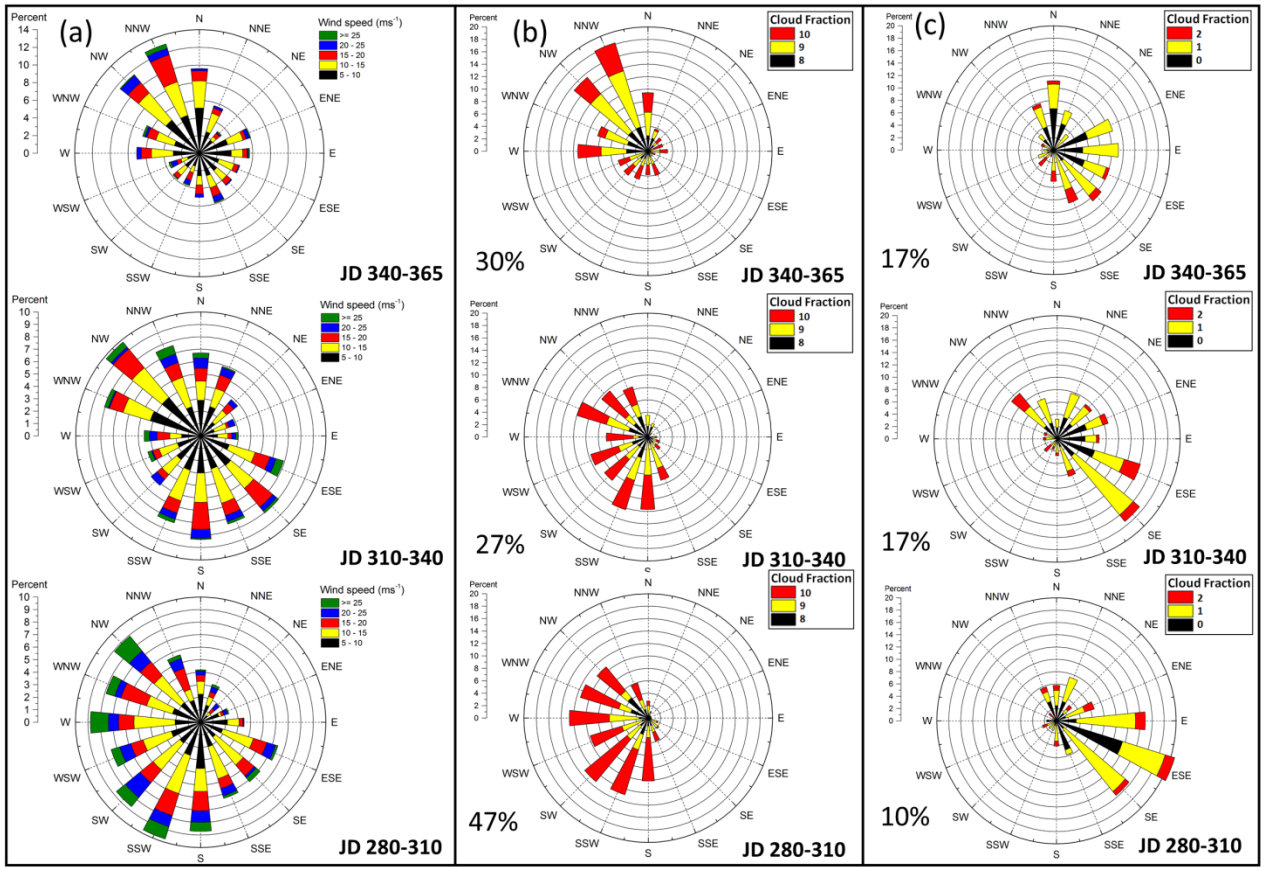

Fig S1. a) Distribution of wind speed and direction at 300 hPa by subseason in 22.5^{o} bins (Note Fig. 1 uses 45^{o} bins), b) Distribution for mostly overcast conditions ($\geq$8/10ths cloud fraction) by 300 hPa wind direction within each subseason. c) Distribution mostly mostly clear conditions ($\leq$2/10ths cloud fraction) by 300-hPa wind direction by subseason. Daily observed average cloud fraction was used: For extreme high and low cloud fraction this provides reasonable assurance of the observed cloud fraction persisted for both rawinsonde launches. Data were restricted to 300-hPa wind speeds > 5 ms^{-1}. Period of data was 1991-2013. The period October-December generally had twice-a-day rawinsondes. Percentages are based on the total number of observations in each interval.

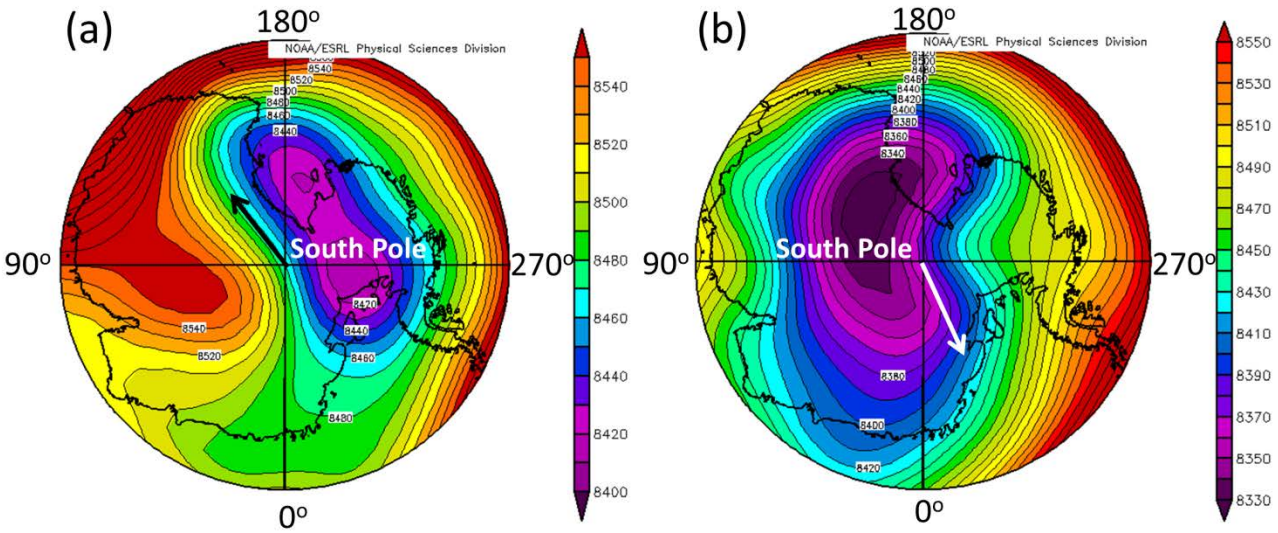

Figure S2. Composite 300 hPa geopotential height patterns for rawinsonde-observed 300 hPa winds (shown in figure) over the South Pole from the NCEP/NCAR Reanalysis from mid-November through December for the period 1991-2010 and wind speeds greater than 10 ms^{-1} and directions (a) between 315^{o} and 360^{o} (61 cases) and (b) between 135^{o} and 180^{o} (75 cases).

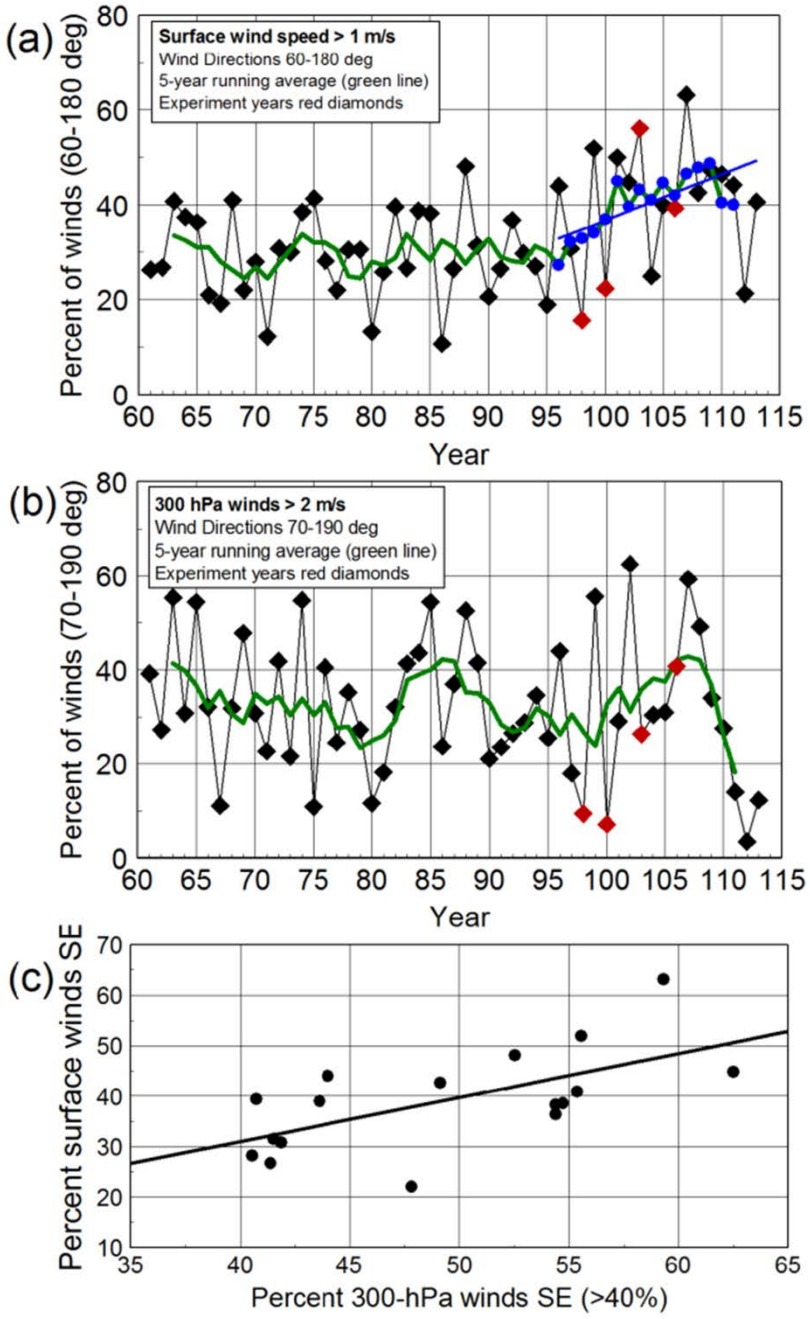

Figure S3. (a) Percent of surface winds from the SE for Late Spring Days 310-340 (60^o-180^o corresponding to higher NO in Figure 3 and wind speed $> 1ms^{-1}$). Five-year running average and experiment years are highlighted. The recent trend is highlighted with r^2=0.6. (b) Same as (a) but for 300-hPa winds. (c) Scatter plot of surface wind percentages for frequency of occurrence of 300-hPa SE wind directions >40%. Least squares linear regression produces r^2=0.4

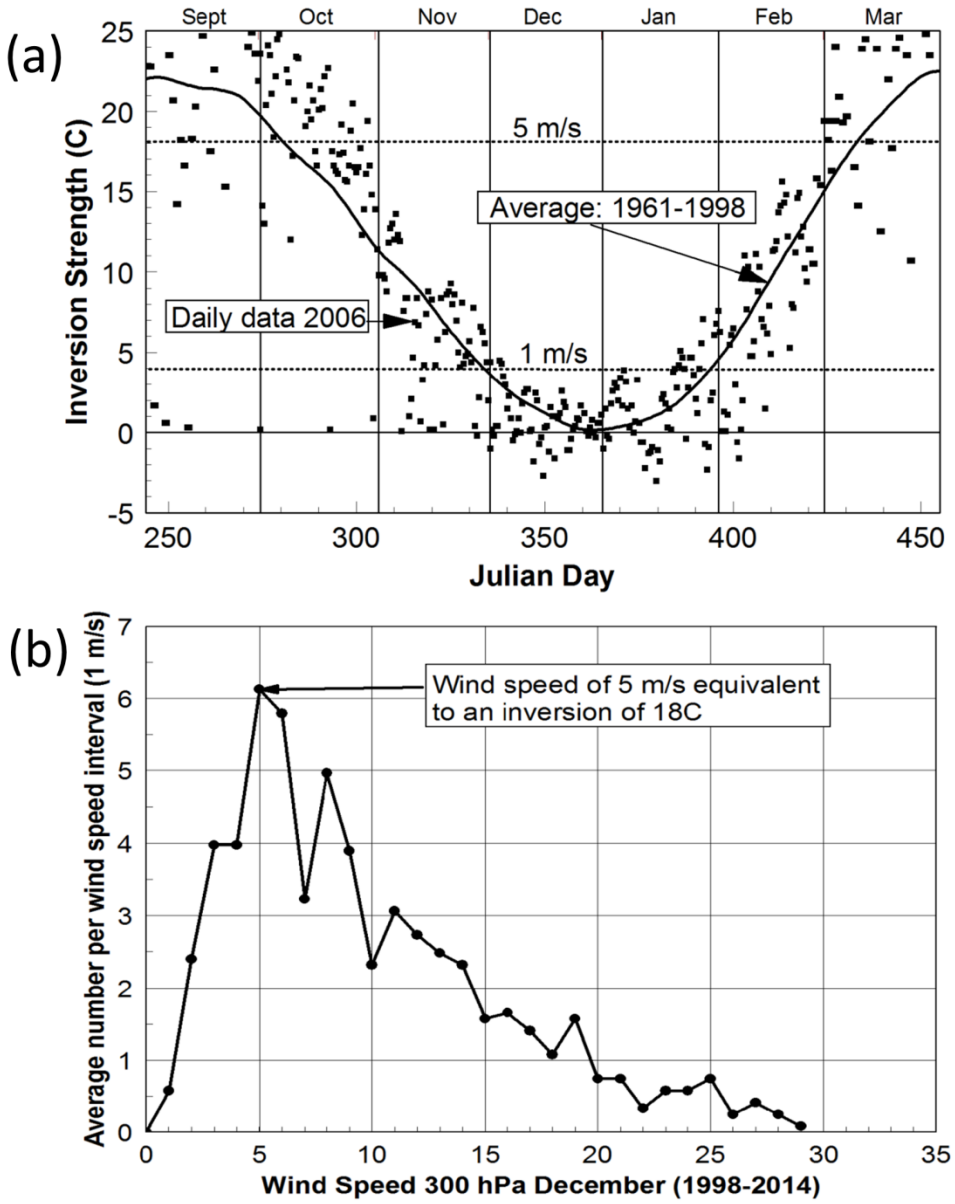

Figure S4. (a) Average inversion strength (derived from rawinsonde data) for 1961-1998 (Neff 1999) together with daily data from 2006. Equivalent geostrophic wind speeds adapted from (Ball 1960). (b)Average number of wind speeds in 1 ms^{-1} intervals at 300 hPa at the South Pole.

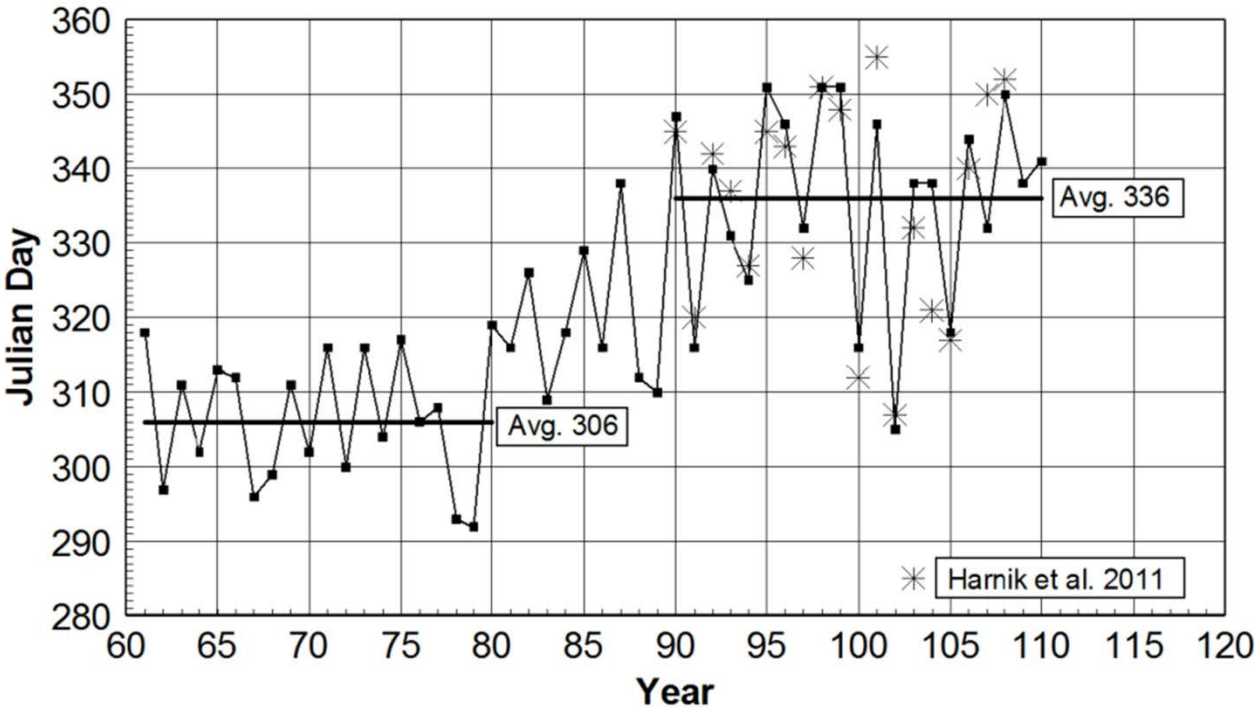

Figure S5. Time of formation of the thermal tropopause over the South Pole from 1961 to 2010 (T200hPa-T300hPa>0.5^{o}C). Averages are shown for 1961-1980 and 1990-2010 with an average delay of 30 days. Asterisks indicate the timing of the breakup at 30–10 hPa from Harnik et al. (2011): as scaled from their Figure 5, the average time is Day 335. (A linear least squares fit shows r^2=0.77 for the period 1990-2009). The differences in timing determined from Harnik et al. (based on time of circumpolar stratospheric winds reversing) and the time of formation of the thermal tropopause (from the SP rawinsonde) is quite reasonable.

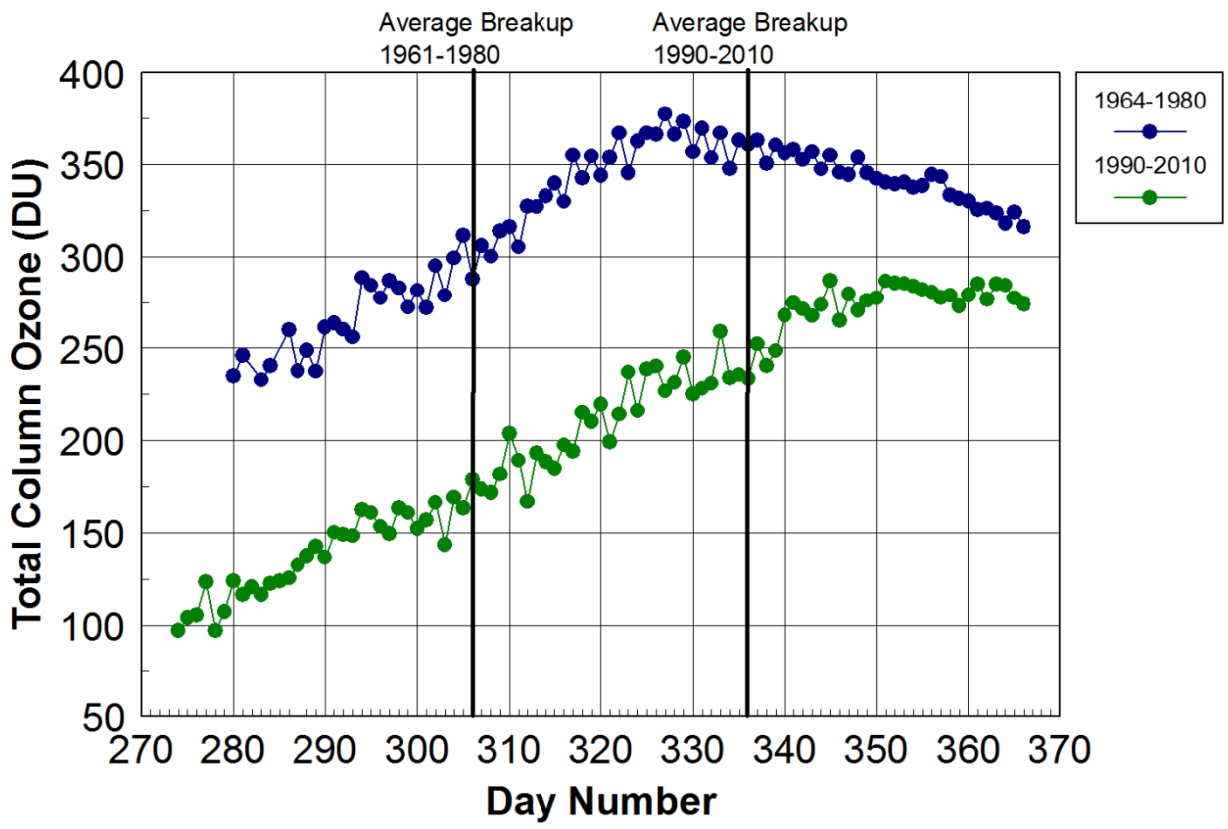

Figure S6. Change in total column ozone measured with a Dobson Ozone spectrophotometer (www.esrl.noaa.gov/gmd/ozwv/dobson/) at the South Pole averaged over day number from 1964 to 1980 and then from 1990 to 2010. The average times of vortex breakup are shown in the figure for both periods.

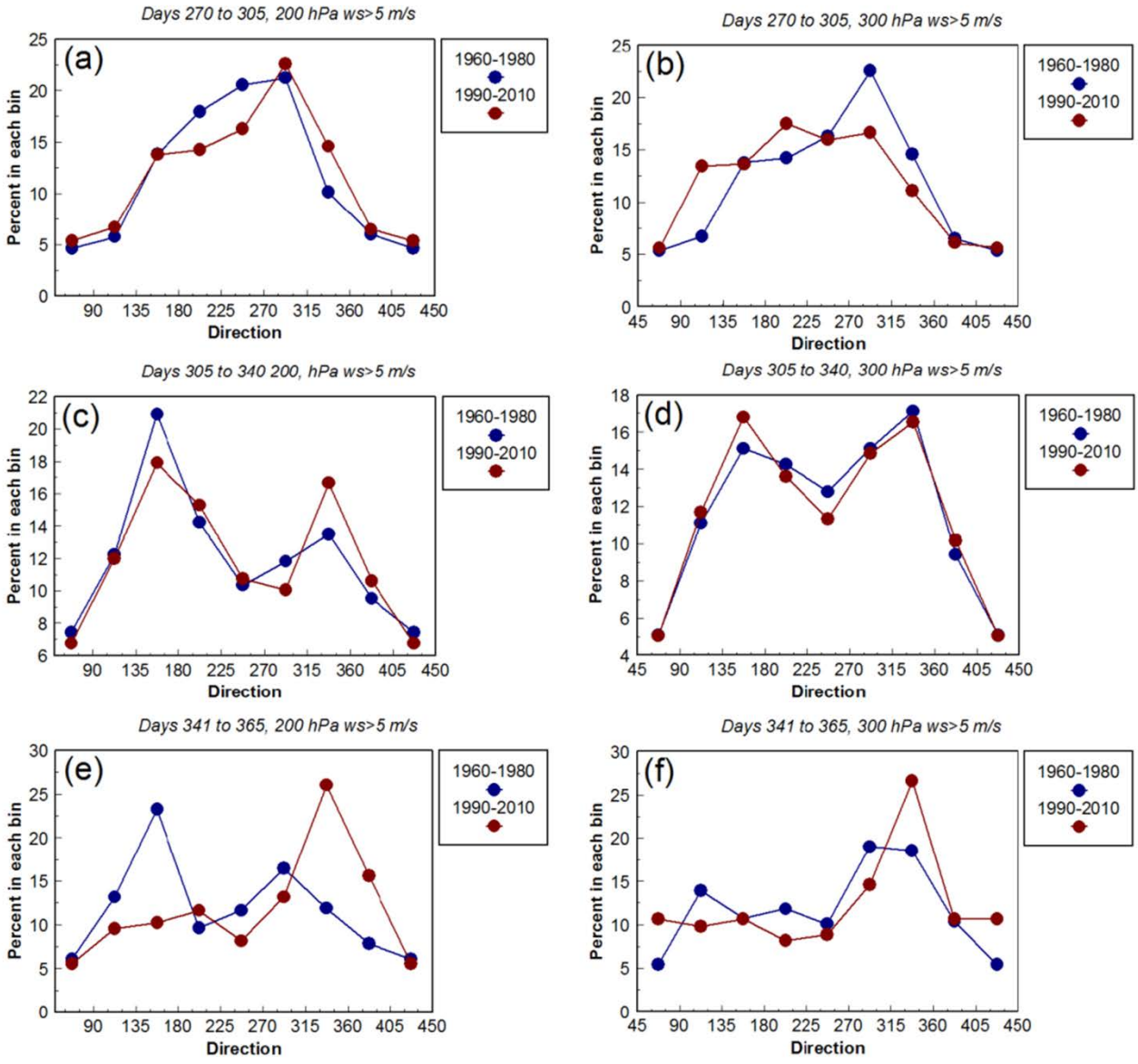

Figure S7. Wind direction distributions at 200 hPa (left) and 300hPa (right) for years 1960-1980 and 1990-2010 and within seasons: Days270-305 (top: a,b), Days 305-340 (middle: c,d) and Days 341-365(bottom: e,f).Wind speeds > 5ms^{-1} only were used. Note that slightly different periods were used compared to those in Figure 1. Note the major difference in distributions for early summer, Days 341-365at 200 hPa. As noted in Neff (1999), the early period is dominated by a strong thermal tropopause above 300 hPa that could decouple winds between 300 and 200 hPa.

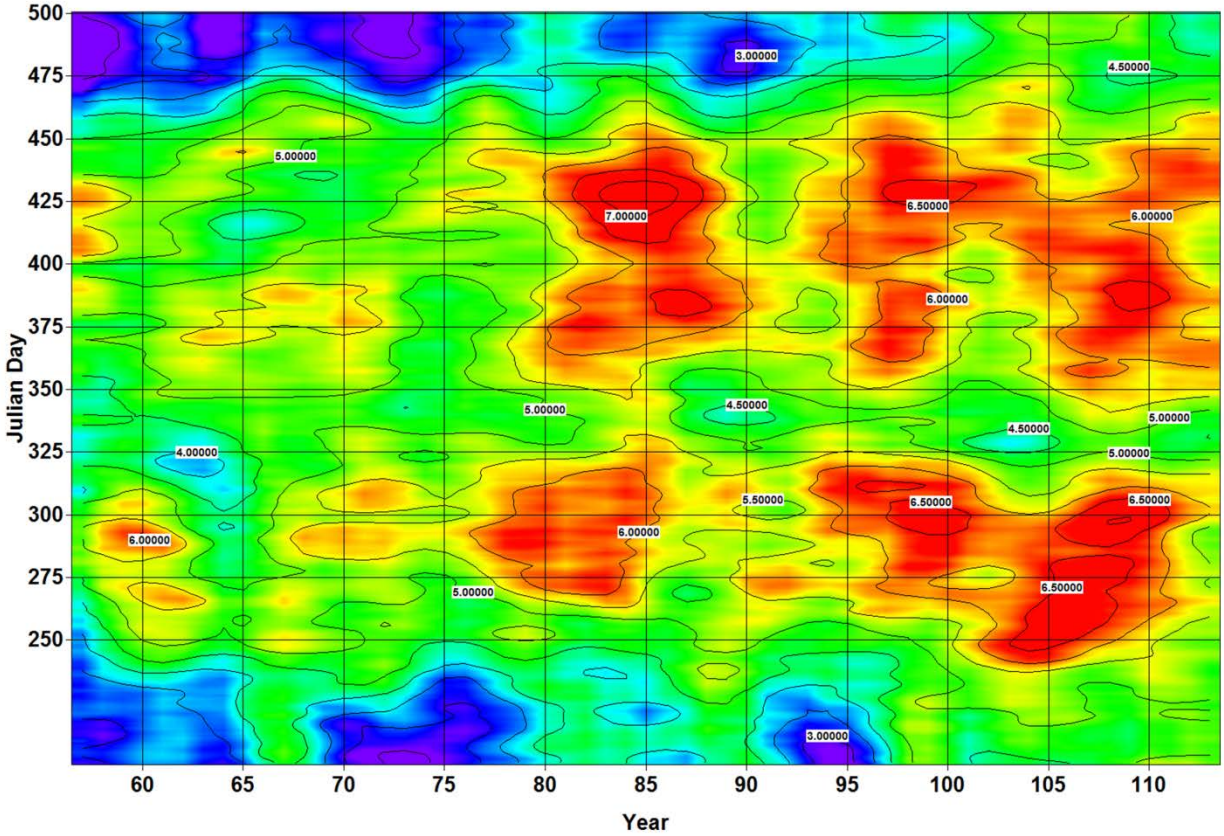

Figure S8. Cloud fraction from average daily observer data 1957 – 2013 (57-113 in figure). Data were smoothed with 14-day filter within each year and then with a five-year tapered filter. Note the decadal time scale variability and the persistent minimum between Days 325and 350. The earlier minimum between 2000 (Year 100) and 2005 (Year 105) corresponds to the earlier average breakup of the polar vortex shown in Fig. S4.

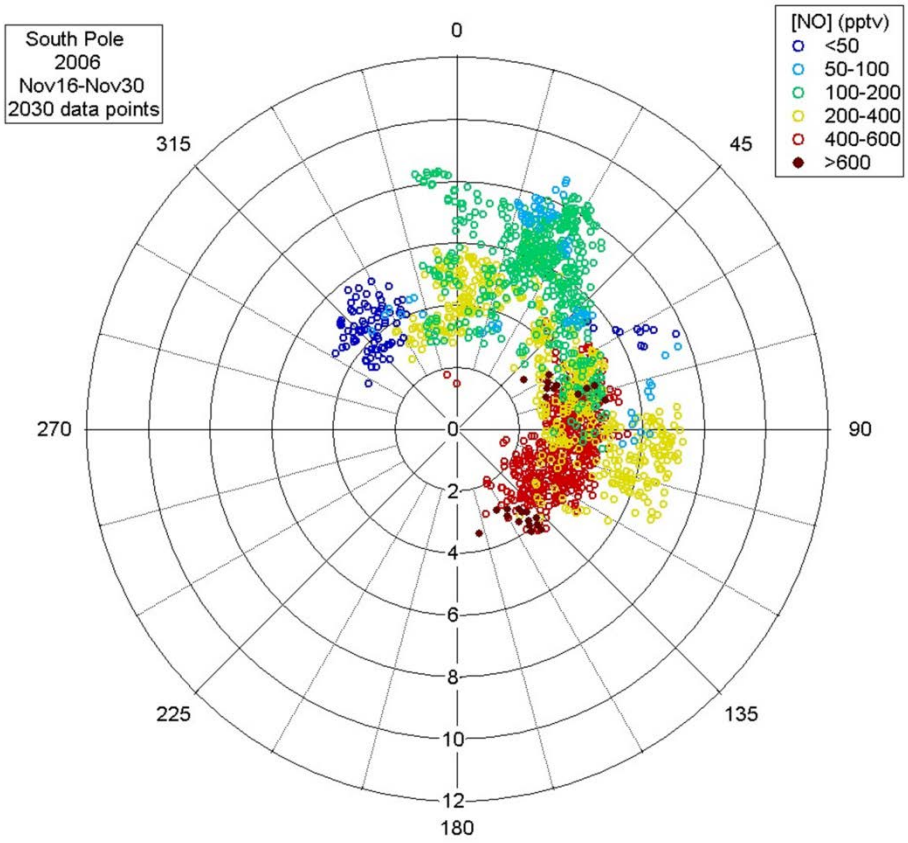

Figure S9. Wind rose plot of 10-min NO versus wind speed and direction for November 16-30 2006. Note the tendency for high NO concentrations to occur with light surface winds from the east-northeast to southeast. The highest NO in this period originates from the direction of the basin shown in Fig. 3.

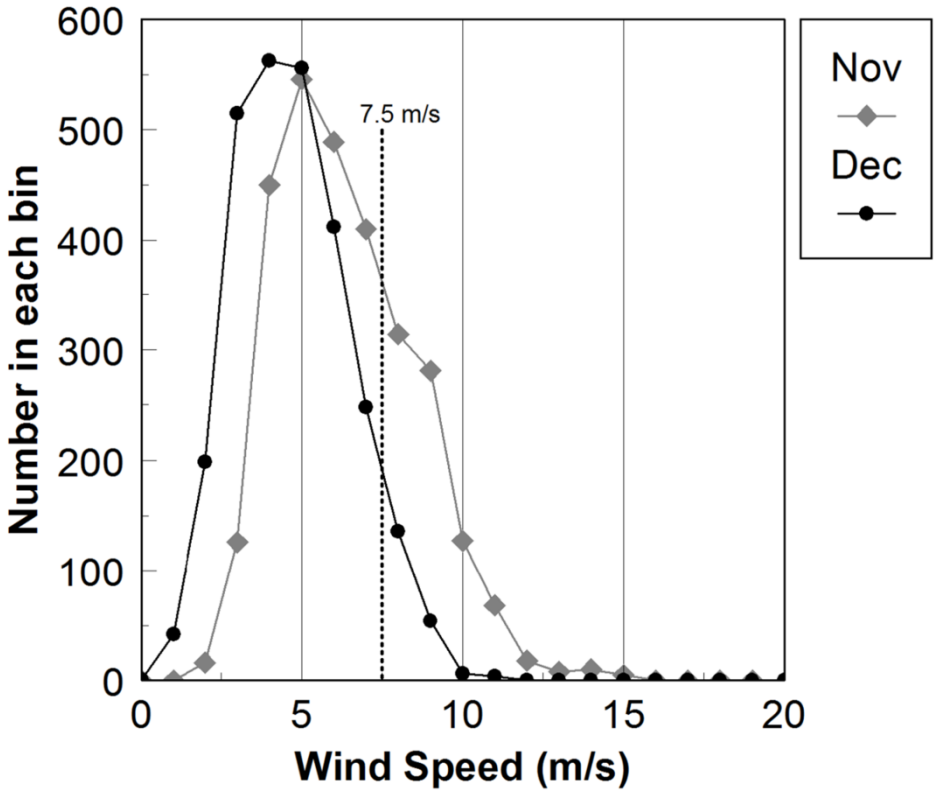

Figure S10. Distribution of one-minute wind speeds in 1 ms^{-1} bins for November (gray) and December (black) of 1998, 2000, 2003, 2006.

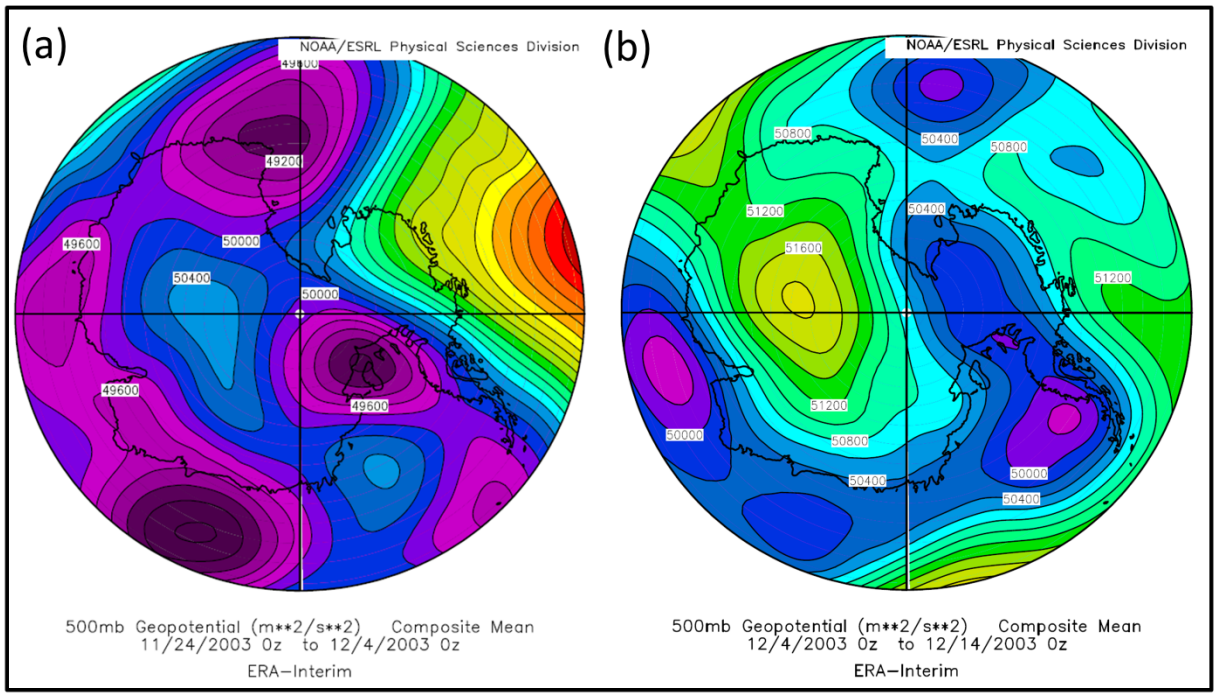

Figure S11. 500 hPa geopotential field for the ten days (a) before and (b) after 12/4/2003. The pattern on the right corresponds to the circulation highlighted by (Arimoto et al. 2008) that emphasizes the counterclockwise circulation dominating the high plateau and conductive to transport from maritime regions.

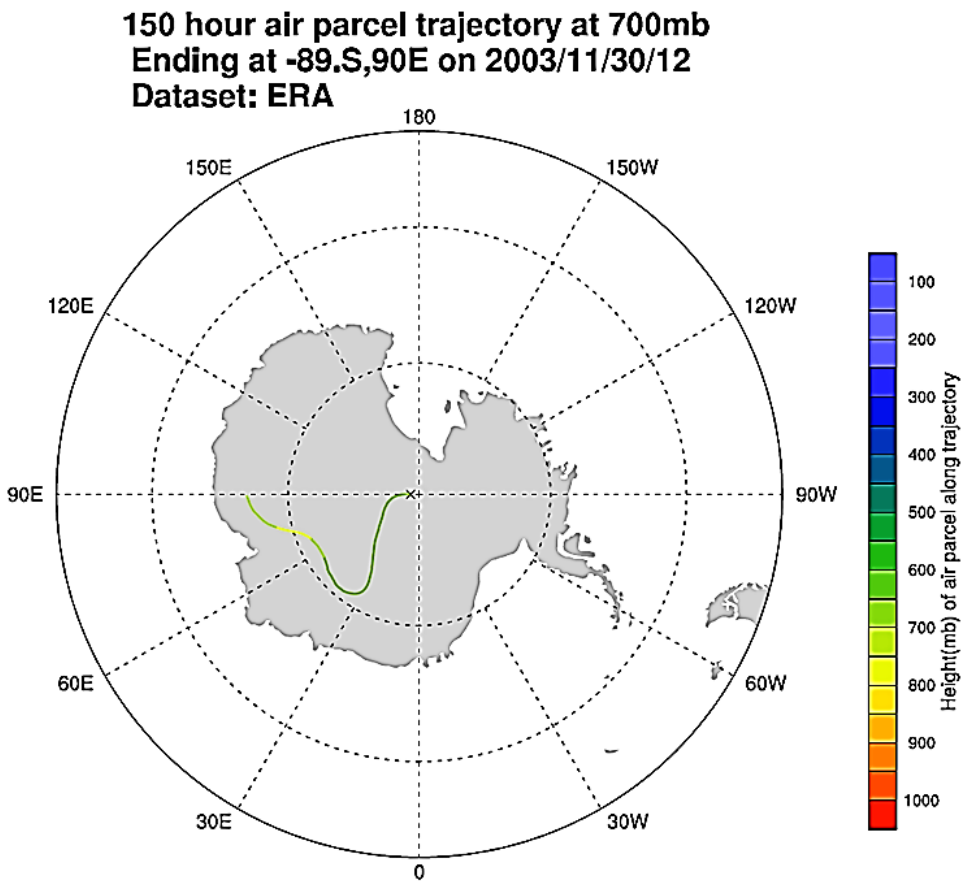

Figure S12. 150 hour back trajectory from ERA-I (Dee et al. 2011) arriving at -89°S, 90°E (AWS Nico) on 11/30/2003 at 12Z at 700 hPa (standard level closest to the elevation at the South Pole). Automatic weather station wind direction at Nico was from 70°E whereas at the South Pole it was 90°E. *Image provided by the NOAA-ESRL Physical Sciences Division, Boulder Colorado from their Web site at http://www.esrl.noaa.gov/psd/. The parcel trajectory software (traj3d) was obtained from the University of Melbourne Parcel Trajectory Software web page (http://www.cycstats.org/trajectories/trajhome.htm).*

Table S1. *Number of hours of winds > 7.5ms^{-1}/total observations each month*

	October	**November**	**December**
1998	91/744	312/717	36/744
2000	150/742	220/668	3/689
2003	140/704	59/647	82/743
2006	55/744	128/720	17/718

Table S2. *Seasonal changes in wind orientation at 300 hPa before and after the final stratospheric warming in 2003 and 2006 (number of rawinsonde observations –not always twice daily).*

	Days 315-340		**Days 340-365**	
	SE	**NW**	**SE**	**NW**
2003	27	14	9	35
2006	23	13	24	18

https://ozonewatch.gsfc.nasa.gov/monthly/SH.html